Transition in Localized Pipe Flow Turbulence

Fernando Mellibovsky,[1] Alvaro Meseguer,[1] Tobias M. Schneider,[2,3] and Bruno Eckhardt[2]

[1]*Departament de Física Aplicada, Universitat Politècnica de Catalunya, 08034, Barcelona, Spain*

[2]*Fachbereich Physik, Philipps-Universität Marburg, D-35032 Marburg, Germany*

[3]*School of Engineering and Applied Sciences, Harvard University, Cambridge, Massachusetts 02138, USA*

(Received 24 March 2009; published 31 July 2009)

Direct numerical simulation of transitional pipe flow is carried out in a long computational domain in order to characterize the dynamics within the saddle region of phase space that separates laminar flow from turbulent intermittency. For Reynolds numbers ranging from Re = 1800 to 2800, a shoot and bisection method is used to compute critical trajectories. The chaotic saddle or edge state approached by these trajectories is studied in detail. For Re $\leq$ 2000 the edge state and the corresponding intermittent puff are shown to share similar averaged global properties. For Re $\geq$ 2200, the puff length grows unboundedly whereas the edge state varies only little with Re. In this regime, transition is shown to proceed in two steps: first the energy grows to produce a localized turbulent patch, which then, during the second stage, spreads out to fill the pipe.

DOI: 10.1103/PhysRevLett.103.054502 PACS numbers: 47.27.nf, 47.20.Ft, 47.20.Lz, 47.27.Cn

Transition to turbulence in pipe flow still remains an open problem of hydrodynamic stability theory. Hagen-Poiseuille or pipe flow (fluid flow through an infinitely long pipe of circular cross-section) is believed to be always stable with respect to infinitesimal perturbations [1] but becomes turbulent in practice [2–5]. It is one of the most fundamental examples of *subcritical* transition to turbulence in fluid dynamics, i.e., transition to turbulence bypassing linear stability (see [6,7] and references therein).

Instability of pipe flow typically occurs for Reynolds numbers above Re $\simeq$ 1750 [4,8]. The standard definition of the Reynolds number in a pipe $\mathrm{Re} = D\bar{U}/\nu$ is adopted, where D is the pipe diameter, $\bar{U}$ is the mean streamwise flow speed and ν is the kinematic viscosity of the fluid. For Reynolds numbers within the range $\mathrm{Re} \in [1750, 2700]$, perturbations can trigger transition to intermittent turbulent spots usually named *puffs*, which coexist with the laminar Hagen-Poiseuille flow [2,5,9]. They can be reproduced reliably in experiments, their averaged properties seem to be independent of the initial condition and their length of about 40–50 radii is preserved during downstream advection. Above Re $\simeq$ 2200–2700, puff structures destabilize, either experiencing a splitting process that leads to a higher number of puffs or, eventually, growing in size and leading to much longer intermittent structures (*slugs*), which are the predecessors of global pipe turbulence.

Much of the recent progress in pipe flow transition understanding is connected to the finding of exact traveling wave solutions to the Navier-Stokes equations. While lower branch traveling waves appear to play an important role in transition, upper branch waves are usually related with the development and eventual sustainment of near-wall turbulence [10–14]. To this date, however, all traveling waves found in fully resolved numerical simulations are periodic with wavelengths of a few pipe diameters and are therefore incapable of explaining the localization and the large-scale intermittency phenomena described above and observed in experiments.

In this Letter we aim to explain the main features of the dynamics of long preturbulent localized states in pipe flow. To this end, we numerically characterize the dynamics on the critical threshold that discriminates relaminarizing orbits from those that lead to turbulent structures. Our goal is to identify the relative attractor within the critical threshold (edge state), and compare its main properties with turbulent structures at the same Re. This allows us to support the expectation that only localized perturbations are needed in order to trigger turbulence and to reveal a two stage process for the formation of spatially extended turbulence in pipe flow. The stable manifold of this localized edge state separates laminar and turbulent flows and can be used to design optimal perturbation strategies.

In cylindrical nondimensional coordinates (r, θ, z), the basic Hagen-Poiseuille solution of the Navier-Stokes problem reads $\mathbf{u}_b = u_b\hat{\mathbf{r}} + v_b\hat{\boldsymbol{\theta}} + w_b\hat{\mathbf{z}} = (1 - r^2)\hat{\mathbf{z}}$. The Navier-Stokes equations for the velocity-pressure $\mathbf{u}$-p perturbation fields are

$$\partial_t\mathbf{u} = -\nabla p + \frac{1}{\mathrm{Re}}\Delta\mathbf{u} - (\mathbf{u}\cdot\nabla)(\mathbf{u}_b + \mathbf{u}) - (\mathbf{u}_b\cdot\nabla)\mathbf{u},$$

$$\nabla\cdot\mathbf{u} = 0, \qquad \mathbf{u}(1, \theta, z; t) = 0,$$

where an adjustable pressure gradient ensures the constant mass-flux constraint and $\Lambda = 100$ is the dimensionless periodic length of the pipe, in radii units. For the spatial discretization we use a solenoidal Petrov-Galerkin spectral scheme with $25 \times 33 \times 193$ radial $\times$ azimuthal $\times$ axial grid points. The solution is evolved using a 4th order linearly implicit method with $\Delta t = 5 \times 10^{-3}$ [15], where we measure time in units of $D/(4\bar{U})$. The scheme has accurately reproduced linear stability analysis results [15] and reliably matched experimental results on transition threshold scaling [16]. Additional computations at even

higher spatial resolution and in a longer domain of $\Lambda = 200$ were carried out to confirm the validity of our edge state simulations.

Starting from a localized pair of rolls, $\mathbf{u}_0 = A(g\sin\theta\hat{\mathbf{r}} + (g + rg')\cos\theta\hat{\boldsymbol{\theta}})e^{-w\sin^2(\pi z/\Lambda)}$, where $g(r) = (1 - r^2)^2$ and $w = 100$ localizes the rolls within about 6 radii, a refinement in the critical amplitude A is carried out via an iterative bisection method, allowing to transiently land on the stable manifold of the critical *edge state* [17,18]. Different algorithms relying on very different time-stepping codes have produced consistent results in the past [13,14,18]. The method only precludes transition and relaminarization, but otherwise allows the flow to freely evolve on the basin boundary, thus evidencing the attracting nature of the edge state [19]. As a relative attractor residing within the critical threshold, its stable manifold separates initial conditions that go turbulent from those that do not.

The trajectory on the edge is always bounded by two neighboring orbits (one leading to turbulence and the other relaminarizing) whose relative euclidean distance is monitored throughout the time evolution. Every time the distance between the two bounding orbits surpasses a prescribed tolerance (10^{-5} in our computations), a new pair of trajectories is found by bisection along the chord connecting the two. Computation is then resumed from the instant of time where the tolerance was violated with the new pair of trajectories. This is illustrated in Fig. 1(a), where the resulting edge trajectory and some of the corresponding relaminarizing and turbulent bounding orbits are represented. Following the critical trajectory for 1000 time units took over a month for each Reynolds number explored within the range $\mathrm{Re} \in [1800, 2800]$, using

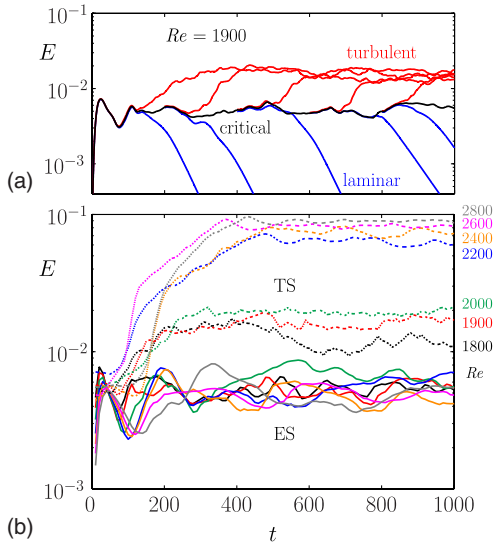

FIG. 1 (color online). a) Energy of turbulent (red) and relaminarizing (blue) trajectories which bracket the edge state (black). The bisection refinements were applied, on average, at time intervals of $\Delta T = 12.8$ time units, never surpassing 40. (b) Energies of the critical (solid) and turbulent (dashed) trajectories for different Re.

4-processor 2.8 GHz SUN machines. The results are shown in Fig. 1(b), where the total perturbation energy associated to trajectories that remain on the edge for arbitrarily long times has been represented as a function of time in $D/4\bar{U}$ units (dubbed ES, solid curves). In the same plot we have included the energies of trajectories that lead to a turbulent *"state"* (labeled TS, dashed curves). For all Re, the energy of critical trajectories remains well below turbulent levels, which allows to apply the discussed approximation method.

In Fig. 2, we show the axial distribution of the axisymmetric and the nonaxisymmetric energy components together with the total energy of both the edge and its corresponding turbulent state (in this case a developed puff) for $\mathrm{Re} = 1900$. The typical energy distribution of a puff can be clearly recognized in Fig. 2(b): an extended leading edge (front), manifested by a slow and mild exponential energy decay in the downstream region, and a sharp trailing edge (rear), characterized by a quick exponential energy drop in the upstream region. In contrast, the edge state, shown in Fig. 2(a), is slightly shorter and characterized by extended interfaces in both the front and rear regions. Both states, however, share in common a fairly axisymmetric front and a strongly nonaxisymmetric rear, as pointed out by the axial distribution of the energy contained in the axisymmetric and nonaxisymmetric modes.

To compare the three-dimensional flow fields of both localized structures, in Figs. 2(c) and 2(d) we represent

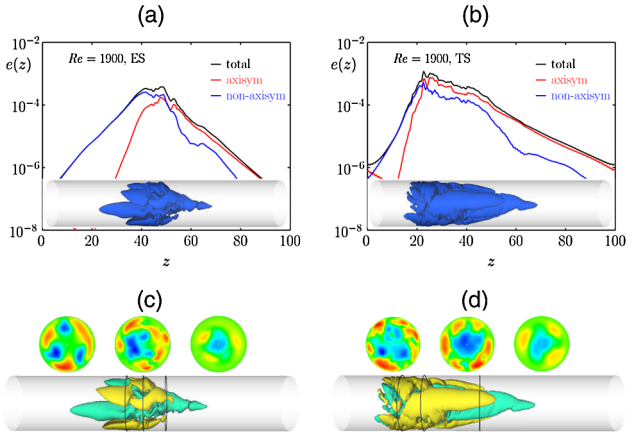

FIG. 2 (color online). Localized edge state (ES) and turbulent state (TS) at $\mathrm{Re} = 1900$. Energy distribution of (a) the localized edge state and (b) a turbulent state. The axial position z is measured in units of the radius. Total energy and the energy contents of the axisymmetric and the nonaxisymmetric components are shown in black, red and blue, respectively. The bottom frame shows energy isosurfaces representing the 3D structure. (c) and (d) show cross-sectional distributions of u_z and $u_z = \pm 0.07$ isosurfaces of the edge state and the turbulent state, respectively. The axial positions of the visualized cross-sections are indicated by rings. Red, green and blue indicate regions where the streamwise flow speed is higher than, similar to or lower than for the corresponding parabolic profile. In all cases the flow direction is from left to right.

instantaneous axial velocity isosurfaces and several pipe cross sections revealing the presence of streaks. The edge state flow field appears as much less complex and preserves higher spatial coherence than the turbulent puff. The threefold azimuthal periodicity evidenced at the rear of the edge state [Fig. 2(c)] is recurrent but not preserved throughout time evolution, although the structure remains simpler than that of the puff at all times.

Having discussed the different dynamical characteristics of the edge state and a turbulent puff at Re = 1900, we now consider higher Re for which pipe turbulence appears in the form of growing slugs instead of equilibrium puffs. Since the states analyzed are chaotic, we report statistical properties, averaged over long time series, rather than properties at given time instants. In Fig. 3(a) we represent time-averaged energies corresponding to edge and turbulent states, asymptotically approached by the critical and turbulent trajectories shown in Fig. 1(b), respectively, for all the Reynolds numbers explored. The error bars correspond to $\pm 2\sigma$. The lowest curve of Fig. 3(a) is the energy of the initial condition (IC) leading to a trajectory that ends up landing on the edge. Discarding the first critical points near the vertical transition threshold, the critical perturbation amplitude corresponding to the initial conditions curve fits the power law $A_c \sim E_{\mathrm{IC}}^{1/2} \sim \mathrm{Re}^{-1.3}$, in agreement with a critical amplitude threshold analysis [20] that explored a wider Re range and was based on global transition via streak breakdown. The edge state energy does not change noticeably within the explored Re range. The critical perturbation energies are much lower than the typical energy of the edge, indicating that its stable manifold bends down to very low amplitudes in some directions of state space. The turbulent energy level is higher, at all Re, than the one associated to the edge, which ultimately makes it possible to track the critical trajectories with the shoot and bisection method described before.

The energy of the turbulent regime experiences a noticeable jump for Re $\geq$ 2200. To better understand this discontinuity, Fig. 3(b), shows the axial length l_z of the structures, defined as the minimal axial extent containing 98% of the axisymmetric energy component in Fig. 2, as a function of Re. These curves clearly show that the turbulent energy surge observed at $2000 \leq \mathrm{Re} \leq 2200$ is associated with the unbounded growth of the turbulent structures, which end up filling the whole domain. This result is in good agreement with former DNS computations [21] that *did not* observe equilibrium puffs for Re = 2200. It differs quantitatively from recent analyses [22], where the computations obtained developed puffs for Reynolds numbers beyond Re = 2200. This can be ascribed to the fact that we are slightly under-resolving puffs (not so with edge states, which are the fundamental object of analysis here). Some checks at very high resolution have shown that while under-resolving puffs leads to altered lifetime statistics as well as to some uncertainty in the prediction of the regime at which unbounded growth of puffs occurs, it does not substantially affect the features that are relevant in the present study. In contrast to turbulence, which starts to expand at about Re $\sim$ 2200, there is no such transition in the edge states branch. The flow structure's length slightly increases with Re but remains bounded, the edge being localized regardless of the dominant turbulent state (puff or slug) to which transition is experienced. The observation of localized edge states even for large Re seems to be generic, as has also been observed in a reduced model that practiced a severe truncation in the azimuthal direction, only allowing for sinusoidal variation [23]. The mean streamwise speed c of the localized states has been plotted in Fig. 3(c). Within the range explored, the advection speed of the edge states does not remarkably change. They always move faster than the mean flow and than the puffs, which travel downstream at about the mean flow velocity with a tendency to slow down as Re is increased.

Finally, Fig. 3(d) depicts the friction factor λ, computed over the structure length l_z, corresponding to both edge and turbulent states. This last plot clearly reveals that the former preserve strong laminar properties, whereas the latter (especially in the puff regime) follow a law which is closer to the one describing fully developed turbulent flow. Beyond Re = 2000, the turbulent branch exhibits a clear change in its friction factor, bending upright and overshooting the λ_{turb} law.

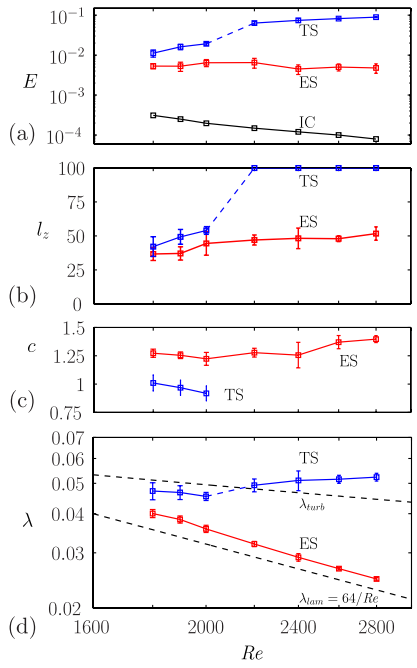

FIG. 3 (color online). Statistical properties of the turbulent states (blue, TS, puffs and slugs) and the edge states (red, ES) as a function of Re. (a) Time-averaged energy of the runs shown in Fig. 1(b). The lowest curve, labeled IC, is the energy of the initial perturbation unfolding the critical trajectory. (b) Length of the ESs and TSs within the explored Re range. (c) Mean axial speed of the ESs and the TS (puffs) in $\bar{U}$ units. (d) Friction factor for the ESs and TSs. For reference, turbulent and laminar friction factors are shown as dashed lines.

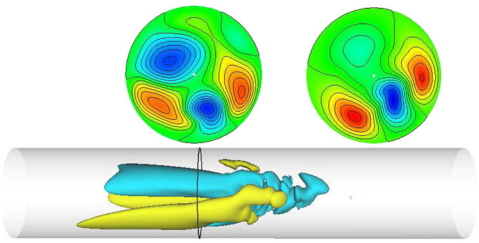

FIG. 4 (color online). $u_z = \pm 0.07$ isosurfaces of the edge state at Re = 2800. Also shown u_z cross-sectional contours at the indicated axial location (top left), to be compared with the traveling wave underlying the short pipe edge state at Re = 2875 (top right).

The simple structure and smoothness of the edge state is preserved within all the explored range and this is clearly evidenced in Fig. 4, for a localized edge state at Re = 2800. This spatially coherent localized structure coexists with global turbulence and thus indicates the different features of turbulence and edge dynamics. This figure shows how the edge states seem to even gain smoothness as Re is increased, the rear gets more and more elongated and the front slightly shorter. The azimuthal simpler spatial coherence is also preserved and clear traces of the traveling wave [14] underlying the edge in a short $5D$ pipe [24] can be recurrently found at the rear of the structure, as can be spotted in the u_z cross sections shown in Fig. 4.

The nature of transition to global turbulence is clarified in Fig. 5, where the energy (E) and axial perturbation length (l_z) have been represented for a destabilizing edge state at Re = 2800. It becomes apparent that transition follows two stages. In a first stage ($t_1 < t < t_2$), a linear instability nucleates in a very short axial region of the ES, and starts growing exponentially in energy but remains narrowly localized in space producing an axial concentration of total energy, which accounts for the apparent shrinking of the structure. The result is a turbulent spot that, in a second stage ($t_2 < t < t_3$), starts a linear unbounded axial expansion. The two stages of the transition process suggest that two distinct instability mechanisms are at work: a first one responsible for the energy increase and a second one causing the spreading in space. While the

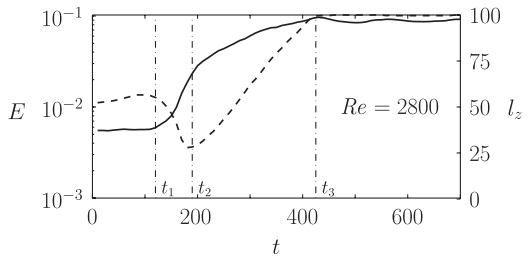

FIG. 5. Time evolution of a destabilizing edge state at Re = 2800: total energy (E, bold line) and structure length (l_z, dashed line). t_1, t_2 and t_3 indicate the beginning of the exponential energy growth, the beginning of the linear growth of axial extent and the saturation to fully developed turbulence, respectively.

first one can be understood through an instability of a rather simple structure of traveling wave type, the second one is perhaps related to the mechanisms at work in other examples of structured turbulence [25,26].

This work has been supported by the Spanish Ministry of Science and Technology, under grants FIS2007-61585 and AP-2004-2235, by the Catalan Government under grant SGR-00024, and by the Deutsche Forschungsgemeinschaft.

[1] A. Meseguer and L. N. Trefethen, J. Comput. Phys. **186**, 178 (2003).
[2] O. Reynolds, Phil. Trans. R. Soc. London **174**, 935 (1883).
[3] A. Darbyshire and T. Mullin, J. Fluid Mech. **289**, 83 (1995).
[4] B. Hof, A. Juel, and T. Mullin, Phys. Rev. Lett. **91**, 244502 (2003).
[5] I. J. Wygnanski and F. H. Champagne, J. Fluid Mech. **59**, 281 (1973).
[6] R. Kerswell, Nonlinearity **18**, R17 (2005).
[7] B. Eckhardt, T. M. Schneider, B. Hof, and J. Westerweel, Annu. Rev. Fluid Mech. **39**, 447 (2007).
[8] J. Peixinho and T. Mullin, Phys. Rev. Lett. **96**, 094501 (2006).
[9] P. R. Bandyopadhyay, J. Fluid Mech. **163**, 439 (1986).
[10] H. Faisst and B. Eckhardt, Phys. Rev. Lett. **91**, 224502 (2003).
[11] H. Wedin and R. R. Kerswell, J. Fluid Mech. **508**, 333 (2004).
[12] C. C. T. Pringle and R. R. Kerswell, Phys. Rev. Lett. **99**, 074502 (2007).
[13] Y. Duguet, A. P. Willis, and R. R. Kerswell, J. Fluid Mech. (to be published).
[14] F. Mellibovsky and A. Meseguer, Phil. Trans. R. Soc. A **367**, 545 (2009).
[15] A. Meseguer and F. Mellibovsky, Appl. Numer. Math. **57**, 920 (2007).
[16] F. Mellibovsky and A. Meseguer, Phys. Fluids **19**, 044102 (2007).
[17] J. D. Skufca, J. A. Yorke, and B. Eckhardt, Phys. Rev. Lett. **96**, 174101 (2006).
[18] B. Eckhardt and T. M. Schneider Eur. Phys. J. B **64**, 457 (2008).
[19] J. Vollmer, T. M. Schneider, and B. Eckhardt, New J. Phys. **11**, 013040 (2009).
[20] F. Mellibovsky and A. Meseguer, Phys. Fluids **18**, 074104 (2006).
[21] H. Shan, B. Ma, Z. Zhang, and F. T. M. Nieuwstadt, J. Fluid Mech. **387**, 39 (1999).
[22] A. Willis and R. R. Kerswell, Phys. Rev. Lett. **100**, 124501 (2008).
[23] A. Willis and R. R. Kerswell, arXiv:0712.2739.
[24] T. M. Schneider, B. Eckhardt, and J. A. Yorke, Phys. Rev. Lett. **99**, 034502 (2007).
[25] D. Barkley and L. S. Tuckerman, Phys. Rev. Lett. **94**, 014502 (2005).
[26] A. Prigent, G. Gregoire, H. Chate, O. Dauchot, and W. van Saarloos, Phys. Rev. Lett. **89**, 014501 (2002).